Radiation Measurements 156 (2022) 106807

Contents lists available at ScienceDirect

Radiation Measurements

journal homepage: www.elsevier.com/locate/radmeas

# Detectors for measurement of microdosimetric quantities

Stefano Agosteo [a,b]

[a] Politecnico of Milano, Dipartimento di Energia, Sezione di Ingegneria Nucleare – CeSNEF, Via La Masa 34, 20156, Milano, Italy
[b] INFN, Sezione di Milano, Via Celoria 16, 20133, Milano, Italy

ARTICLE INFO

*Keywords:*
Microdosimetry
Hadron therapy
TEPCs
Silicon detectors
GEM detectors
Diamond detectors

ABSTRACT

Microdosimetric quantities have been used for assessing the radiation quality of hadron therapy fields since long. They are stochastic quantities whose distributions depend on the fluctuations of energy deposition in cellular and/or sub-cellular structures. The present work overviews the detectors which are used mainly for assessing the radiation quality of hadron therapy fields (protons and carbon ions), discussing their advantages and limitations based on the author's experience. The microdosimeters which are described and discussed herein are, in particular, tissue-equivalent proportional counters (TEPCs), gas detectors based on gas-electron multiplication (GEMs), silicon and diamond detectors.

## 1. Introduction

In the last two decades, the interest in the application of microdosimetry for radiation quality assessment of hadron therapy fields has grown (e.g., Rosenfeld et al., 2002; De Nardo et al., 2004a, 2004b; Wroe et al., 2009; De Nardo et al., 2010; Agosteo et al., 2010, 2011a; Lindborg and Nikjoo, 2011; Tran et al., 2018; Colautti et al., 2018a, 2018b; Mazzucconi et al., 2019a; Bianchi et al., 2020a, 2020b; Bortot et al., 2020; Colautti et al., 2020a, 2020b; Conte et al., 2020; Guardiola et al., 2020). Radiation quality is closely related to the linear energy transfer (*LET*), which, in the case of hadron beams varies across the depth-dose distribution of the therapeutic beam, resulting in a different biological and clinical response.

It should be stressed that microdosimetry is based on stochastic quantities which express the fluctuations of energy deposition in micrometric and sub-micrometric structures, while the *LET* is a non-stochastic quantity giving the mean energy transferred in an infinitesimal part of the particle path.

A significant quantity for expressing biological effects of radiation is the *relative biological effectiveness (RBE)*, which accounts for the response to different radiation fields in a cell culture:

$$RBE = \frac{D_{ref}}{D} \tag{1}$$

where $D$ is the absorbed dose required to produce a given effect (e.g., a given survival fraction) on the irradiated system and $D_{ref}$ is the absorbed dose from the reference radiation field producing the same biological effect in the same cell system. Generally, although there is no international agreement about this issue, the reference radiation field is constituted by 150 kV X rays or by gamma rays from $^{60}$Co decay. The *RBE* depends on the absorbed dose, cell type and biological end-point (Nikjoo and Lindborg, 2010). The *RBE* dependence on the LET was observed in many cell systems, but this is not a univocal relation, since different particles may show the same LET value, but a different track structure leading to a different effect.

Radiation damage at the DNA level is closely linked to the particle track structure. The unrestricted LET does not give any information about the track structure, which also consists of delta-ray electrons. The use of the LET while neglecting the particle track structure can be a reasonable approximation for low-LET radiation for which the therapeutic dose relates to hundreds or thousands of particles traversing a single cell (Paganetti, 2014). The effects of radiation can be described more accurately in a cellular or sub-cellular volume by microdosimetric quantities or individual particle tracks (Paganetti, 2014). Physical quantities more correlated to the particle track structure are defined in nanodosimetry (De Nardo et al., 2002; Grosswendt et al., 2014; Conte et al., 2015).

The microdosimetric quantities are at the basis of the microdosimetric kinetic (MKM, Hawkins, 1996, 1998) model, which is applied for treatment planning in hadron therapy.

New accelerator-based neutron sources for boron neutron capture therapy (BNCT) are in operation since the last decade (Kreiner et al., 2016; Grosso et al., 2016; Suzuki, 2020) and others are being planned, like the one to be built at the National Centre for Oncological Therapy (Centro Nazionale di Adroterapia Oncologica, CNAO, Pavia, Italy) in the

*E-mail address:* stefano.agosteo@polimi.it.

https://doi.org/10.1016/j.radmeas.2022.106807
Received 28 March 2022; Received in revised form 24 May 2022; Accepted 31 May 2022
Available online 3 June 2022

next two years. The BNCT irradiation field is complex, since it is composed by different radiation fields (thermal or epithermal therapeutic neutrons, fast neutrons, gamma rays). Microdosimetry can be fundamental for assessing the radiation quality in BNCT fields and some tissue-equivalent proportional counters (TEPC) were constructed for this purpose (e.g, De Nardo et al., 2004c; Moro et al., 2006). However, these microdosimeters can hardly model the *RBE* dependence on the localization of the $^{10}$B or the $^{157}$Gd compound in a cell, which can only be assessed through radiobiology. A fairly wide variation of the RBE values assessed in different BNCT reactor-based therapeutic fields through the *in vivo* irradiation of a reference biological system (crypt regeneration in mice) was observed by Gueulette et al. (2004, 2006). The reason of this variation can be ascribed to the different reactor types and beam shape assemblies (BSAs) which are used for tailoring the neutron (fission neutron as a source) energy distribution and the gamma ray dose to the therapeutic requirements. A radiation quality variation can also be expected for accelerator-based neutron sources, since different nuclear inelastic reactions are used for neutron generation (e.g., from lithium or beryllium targets bombarded with protons of different energies) and different materials are employed for the BSAs.

Microdosimetry can play a fundamental role for the radiation quality assessment of hadron therapy fields. As discussed in the present work, the radiation quality can be expressed either through average microdosimetric quantities or the microdosimetric relative biological effectiveness ($RBE_\mu$), which in turn can be obtained either from the MKM model or by folding the microdosimetric spectrum with a weighting function from radiobiological data.

This work describes different types of microdosimeters which are used for this purpose, their advantages and limitations, by basing mainly on the author's experience in the field.

## 2. Microdosimetric quantities for radiation quality assessment

The microdosimetric quantities are defined in the ICRU publication no. 36 (ICRU, 1983). The fundamental stochastic quantities are the specific energy $z$ and the lineal energy $y$, defined as:

$$z = \frac{\varepsilon}{m} \tag{2}$$

$$y = \frac{\varepsilon}{\bar{\ell}} \tag{3}$$

where $\varepsilon$ is the imparted energy (which is a stochastic quantity), $m$ the mass contained in a volume (site) and $\bar{\ell}$ the mean chord length in a volume. Lineal energy is defined for a single energy deposition event. The unit of the specific and the lineal energy is the gray (Gy) and the keV $\mu m^{-1}$, respectively. Only the lineal energy will be accounted for in the following, since usually the radiation quality is assessed in terms of it.

The probability density $f(y)$ is also referred as lineal energy distribution or frequency distribution: $\int_{y_1}^{y_2} f(y)dy$ gives the fraction of events in a given interval from $y_1$ to $y_2$. The dose distribution $d(y)$ is usually referred as *microdosimetric distribution*: $\int_{y_1}^{y_2} d(y)dy$ expresses the fraction of absorbed dose in a given interval from $y_1$ to $y_2$. It should be remembered that both the distributions refer to a single event only. The expectation values of the lineal energy and the dose distribution (frequency-mean lineal energy and dose-mean lineal energy, respectively) are:

$$\bar{y}_F = \int_0^\infty y f(y)dy \tag{4}$$

$$\bar{y}_D = \int_0^\infty y d(y)dy \tag{5}$$

$d(y)$ and $f(y)$ are related by the following equation:

$$d(y) = \frac{y f(y)}{\bar{y}_F} \tag{6}$$

And therefore:

$$\bar{y}_D = \frac{1}{\bar{y}_F}\int_0^\infty y^2 f(y)dy \tag{7}$$

For gas detectors, such as TEPCs, a tissue site of micrometric dimensions can be simulated by a macroscopic cavity filled with a low-pressure gas, if the energy loss of charged particles traversing the cavity is the same as in a tissue site traversed with an equivalent trajectory. For a tissue sphere $d_t$ in diameter and a gas sphere $d_g = kd_t$ in diameter, the condition is:

$$\Delta E_t = \left(\frac{S}{\rho}\right)_t \rho_t d_t = \left(\frac{S}{\rho}\right)_g \rho_g d_g = \Delta E_g \tag{8}$$

where $\Delta E_t$ and $\Delta E_g$ are the mean energy losses of charged particles in tissue and in the gas, respectively, $(S/\rho)_t$ and $(S/\rho)_g$, are the mass stopping powers of charged particles in tissue and in the gas, respectively and $\rho_t$ and $\rho_g$ the tissue and gas density. The above equation has been written for a particle traversing the site along its diameter, but it holds for any trajectory traversing the site. If the chemical composition of gas and tissue are the same (practically, if the gas is tissue-equivalent) and if the stopping powers are independent of density:

$$\rho_g = \frac{\rho_t}{k} \tag{9}$$

and, by assuming that the tissue density is equal to 1 g $cm^{-3}$:

$$\rho_g = \frac{1\ g\ cm^{-3}}{k} \tag{10}$$

The site size can be modified by adjusting the gas pressure in a TEPC of given dimensions. The accuracy of the gas pressure value reflects in that of the size of the simulated site. In a proportional counter, the zone inside which charge multiplication occurs is very close to the anode. Below a given pressure, this zone extends towards the cathode leading to a loss of energy resolution and thus limiting the smallest site size. Of course, the site size of solid-state microdosimeters is determined by the dimensions of their sensitive volume, which cannot be modified. Microdosimetric spectra from different detectors should be compared for similar site sizes, thus correcting for tissue- and shape-equivalence (Section 4.2).

It should be noted that the detectors which are described in this work measure directly ionization (in a gas, silicon or diamond). The collected charge from a single event is transformed and shaped into a voltage pulse by a charge preamplifier connected to an amplifier. The pulse voltage amplitude is then related to imparted energy through the *calibration* of the detection system. Generally, only detectors operating in pulse-mode can be employed for measuring the imparted energy from single events and its frequency distribution (through a multi-channel analyser). The imparted energy can be related to lineal energy by dividing by the mean chord length of the detector's sensitive volume, which, in turn, should possess well-defined dimensions (this may not be true for silicon detectors).

The microdosimetric distributions contain most of the information about the radiation quality of a therapeutic beam. Fig. 1 shows a set of microdosimetric distributions measured at different positions along the depth-dose profile of the spread-out Bragg peak (SOBP) from 62 MeV protons delivered at the INFN-CATANA facility (Istituto Nazionale di Fisica Nucleare, INFN; Laboratori Nazionali del Sud, LNS, Catania, Italy) for treating eye tumours. These measurements were performed with an avalanche-confinement tissue-equivalent proportional counter (TEPC, Section 4.1) simulating a 300 nm site. The distributions shift towards

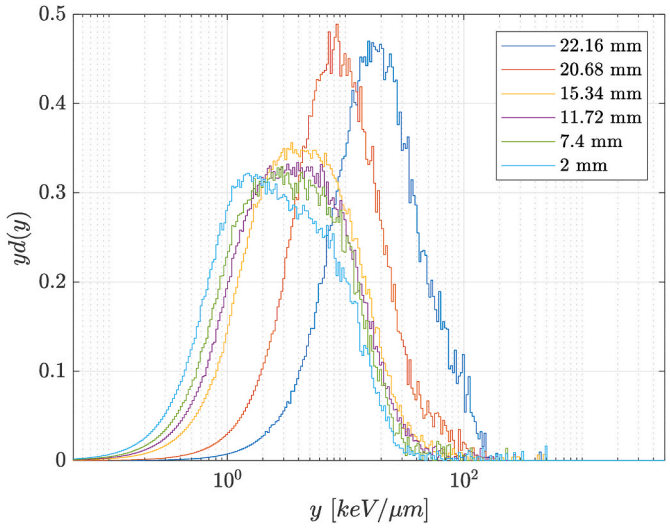


**Fig. 1.** Microdosimetric distributions for different positions across the CATANA proton SOBP measured with an avalanche-confinement TEPC in a simulated 300 nm site (from Mazzucconi et al., 2019a).

higher lineal energy values with increasing depth and, therefore, proton *LET*. This shift indicates a change in the radiation quality since the distributions are seated on higher lineal energy values, thus signalling an *LET* increase of the radiation field. The interpretation of the microdosimetric spectra could not be straightforward for non-experts in microdosimetry. Therefore, it is advantageous and common practise to characterize radiation quality by average quantities rather than through distributions.

The dose-mean lineal energy $\bar{y}_D$ is one of the microdosimetric quantities which can be employed for expressing the radiation quality. Fig. 2 shows the $\bar{y}_D$ at different positions along the depth-dose profile of the CATANA proton SOBP measured with the same avalanche confinement TEPC for different simulated site sizes. The $\bar{y}_D$ trend signals clearly the radiation quality increase with depth. In other words, a higher $\bar{y}_D$ value is related to a higher radiation quality, at least below the values for which the overkilling effect becomes predominant.

Another quantity employed for expressing the radiation quality of therapeutic beams is the microdosimetric $RBE_\mu$ (De Nardo et al., 2004b). It can be assessed by folding the dose probability density *d(y)* with an

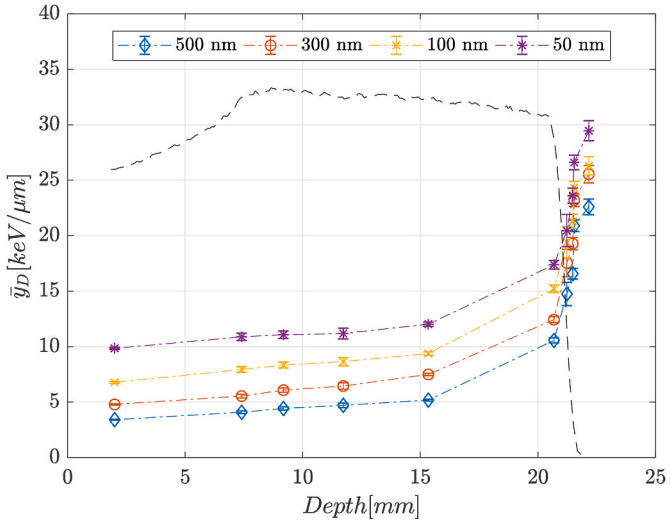


**Fig. 2.** Dose-mean lineal energies and uncertainty bars for different simulated site sizes and for different positions across the SOBP. The dashed line indicates the depth-dose curve of the proton SOBP (from Mazzucconi et al., 2019a).

RBE-weighting function *r(y)*:

$$RBE_\mu = \int_0^\infty r(y)d(y)dy \tag{11}$$

It should be stressed that this is not an estimate of the RBE. It should also be remembered that RBE is not a unique and not a physical quantity and therefore it cannot be measured directly with an instrument. RBE is referring to a particular biological endpoint (such as, e. g. a particular value of clonogenic survival probability) and can be assessed only through radiobiological experiments by irradiating cell cultures. It depends strongly on the type of irradiated cells, the dose, the physiological conditions of the sample, etc. The $RBE_\mu$ is a parameter which can only be useful for expressing the radiation quality. It is assessed through the weighting function *r(y)* which refer to radiobiological effects induced in specified samples under specified irradiation conditions and to microdosimetric spectra measured inside simulated sites of specified dimensions. The *r(y)* function was first derived by (Loncol et al., 1994) from RBE values ($^{60}$Co as reference radiation) for early effects (intestinal crypt regeneration) in mice at 8 Gy and from microdosimetric spectra measured in 2 μm simulated site for photon, proton and fast neutron fields (Colautti et al., 2020b). Another weighting function *r(y)* was proposed more recently by Parisi et al. (2020) from RBE literature data for the 10% survival of V79 Chinese hamster lung fibroblasts. For calculating this weighting function, radiation transport was simulated with a Monte-Carlo code for a wide set of ions from protons up to $^{238}$U, thus completing the data set by Loncol et al. (1994).

It should be mentioned that the $RBE_\mu$ could be a more straightforward and "user-friendly" quantity for expressing the radiation quality also for non-experts in microdosimetry.

The $RBE_\mu$ can also be assessed through the microdosimetric kinetic model (MKM, Hawkins, 1996, 1998) or its modified version (MMKM, Chen et al., 2018) for heavy ions. The model is based on $\bar{y}_D$ and parameters from radiobiology. Kase et al. (2006) accounted for the saturation effect at high LET values by using a corrected expression for the $\bar{y}_D$ and an empirical saturation parameter $y_0$ above which the overkilling effect becomes important. The MMKM model by (Chen et al., 2018) considers the LET dependence of the double strand yield and of the $\beta$ parameter (assumed to be constant in the original MKM) for heavy ions by fitting data from radiobiology experiments.

For assessing the radiation quality in radiotherapy, the normalized dose-mean lineal energy $\bar{y}_D^*$ was proposed by Lindborg et al. (2013). That work showed that, by reducing the simulated volume down to about 10 nm, there is a roughly linear correlation between clinically reported RBE values observed in fractionated radiation therapy and early reacting tissues and the $\bar{y}_D$ normalized to that from $^{60}$Co γ-rays. This was observed when the α/β ratio used in the linear quadratic relation was the same at both radiation qualities. When those ratios differ, a correction was applied.

Following this approach, and by assuming the dose mean lineal energy value at 2 mm depth in water for each simulated site as the reference, the following normalized dose mean lineal energy is defined:

$$\bar{y}_D^*(x) = \frac{\bar{y}_D(x)}{\bar{y}_D(2\ mm)} \tag{12}$$

where $x$ is the depth in water.

An example of the application of the $\bar{y}_D$ and the $RBE_\mu$ can be found in (Mazzucconi et al., 2019a), where the microdosimetric distributions shown in Fig. 1 are analyzed. Since the avalanche-confinement TEPC employed in (Mazzucconi et al., 2019a and Section 4.1 of the present work) is capable of measuring down to nanometric sites, a comparison was made between this defined $\bar{y}_D^*$ and the $RBE_\mu$ values assessed by De Nardo et al. (2004b) from the weighting function from (Loncol et al., 1994). It was found that the smaller was the site size, the smaller was the variation of the $\bar{y}_D^*$ between the proximal and distal depths and thus the

trend of the normalized dose mean lineal energy became gradually in agreement with the $RBE_{\mu}$ one. The best agreement between the two curves was achieved for a 50 nm site (Fig. 3).

## 3. Radiation quality assessment in hadron therapy: detector features

As already mentioned, dose-mean lineal energy $\bar{y}_D$ and $RBE_{\mu}$ can be determined from the lineal energy distribution $f(y)$ acquired with a microdosimeter operating in pulse mode. However, the high intensity of the treatment beams may hinder the use of TEPCs of standard dimensions, because of pulse pile-up. TEPCs with cavities of small dimensions (of the order of a few mm) have been built for alleviating this problem. Different types of millimetric-size TEPCs are described further below. It should be stressed that the counting rate referring to the exposure of millimetric size detectors (even silicon detectors) to clinical hadron therapy fields can be of the order of $10^6$ $s^{-1}$ and more, thus generating a too high pile-up rate obscuring the frequency distribution of single events. Therefore, in most cases, measurements can be performed by decreasing the therapeutic beam current to values which are not employed in the clinical practice. It should be mentioned that the maximum counting rate for a mini-TEPC is in the range 5–50 $\times$ $10^3$ $s^{-1}$ (Bianchi et al., 2021).

An alternative approach consists in assessing $\bar{y}_D$ through the variance method (ICRU, 1983) with a microdosimetric ion chamber operating in current mode (thus avoiding any effect related to the pulsed time structure of the radiation field). The method relies on the higher variance of the charge collected by an ionization chamber in a fixed time interval as the particle stopping-power increases. In other words, if the dose rate is constant during the measurement, a low number of high LET particles is necessary to generate the same amount of charge (dose) which would have been collected with low LET radiation. A high variance is then related to high LET radiation and a high average radiation quality of the beam. The dose-mean lineal energy is evaluated with the following expressions (ICRU, 1983; Hsu et al., 2008):

$$\bar{y}_D = V_r \frac{\bar{J} W}{\bar{l}} \tag{13}$$

$$V_r = \frac{\overline{J^2} - \bar{J}^2}{\bar{J}^2} \tag{14}$$

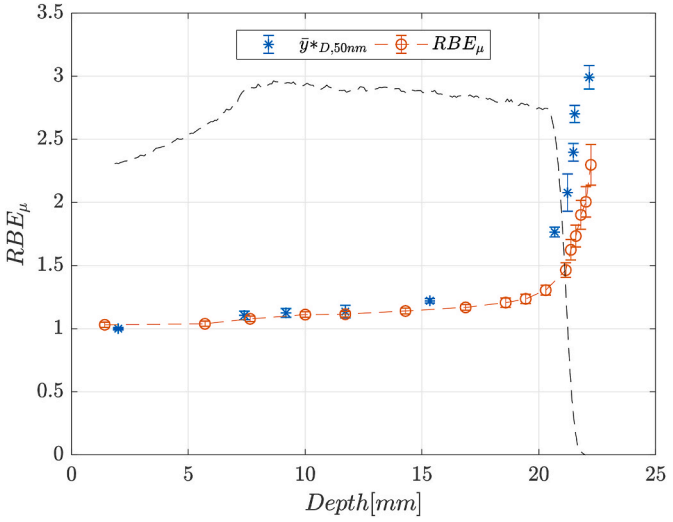


**Fig. 3.** Comparison between the normalized $\bar{y}_D^*$ at 50 nm and the microdosimetric RBE (De Nardo et al., 2004b) as a function of the depth in a PMMA phantom. The dashed curve shows the relative variation of the dose along the SOBP (from Mazzucconi et al., 2019a).

where $J$ is the average charge collected by the ionization chamber with no gas gain, $W$ the mean energy expended per ion pair and $\bar{l}$ the mean chord length of the simulated micrometric site. Hsu et al. (2008) used a spherical ionization chamber with walls made of A-150 plastic connected to a specialized amplifier (using commercial integrated circuits) to assess the radiation dose and quality of different photon fields and of a mixed photon-neutron field from a research reactor through the variance method. Their detection system has been demonstrated to be very useful and robust for assessing on-line the radiation quality of intense radiation beams.

It should be mentioned that the radiation quality can also be assessed with recombination chambers (Zielczyński et al., 1996; Zielczyński and Golnik, 1994). These ionization chambers are based on columnar recombination of the ions produced in the filling gas by charged particles. Columnar recombination depends on the ionization density and therefore on the particle *LET*.

The detector dimensions can also be critical for measurements of hadron therapy beams delivered with active scanning systems. For example, the beam cross section of the CNAO beam is about 1 cm FWHM. This hinders the use of centimetric TEPCs which would be partially irradiated by modifying the expected chord length distribution. Moreover, centimetric TEPCs would also suffer from the pile-up effects mentioned above for their higher efficiency.

The electronic noise can obscure the microdosimetric spectra at low $y$ values especially for silicon detectors with a thin sensitive area. The low lineal energy threshold can be of a few keV $\mu m^{-1}$ for silicon detectors (up to about 10 keV $\mu m^{-1}$ for the single stage silicon telescope described in Section 4.2), since their capacitance is fairly high (up to 1 nF for the single stage silicon detector described in Section 4.2). This may hinder the measurement of the whole microdosimetric spectrum for low *LET* radiation (e.g., protons in the proximal part of the Bragg peak). TEPCs usually show lower lineal energy thresholds below 1 keV $\mu m^{-1}$ (Bianchi et al., 2021), but in general the measured spectrum is extrapolated down to 0.01 keV $\mu m^{-1}$. Bianchi et al. stressed that, by neglecting a significant part of the microdosimetric spectrum below the threshold (i.e., by not extrapolating it down to lower values), the microdosimetric average values (such as $\bar{y}_D$) can be overestimated up to 50% (e.g., for 62 MeV protons at low depths in the proximal part of the Bragg peak). These deviations can be reduced by extrapolating linearly down to 0.01 keV $\mu m^{-1}$. Bianchi et al. (2021) also observed that when the $RBE_{\mu}$ is assessed through the weighting function method (equation (11)), the deviation between the use of extrapolated and non-extrapolated spectra, is less critical (lower than 5%), apart from some cases in the distal part of carbon ion Bragg peak. The same authors stressed that the deviation might be higher when using the MKM model, which is based on microdosimetric average quantities.

The detector calibration is a non-trivial issue, since the low gas pressure (for gas detectors) and/or the very small sensitive volume hinder the full energy absorption of the radiation emitted by a calibration source. Usually, TEPCs with a centimetric sensitive volume house a collimated alpha-particle ($^{244}Cm$) calibration source. The detector calibration accounts for the energy deposited inside the gas and the loss due to delta-rays escaping from the sensitive volume. However, these calibration sources can limit the transportability of the detector since legislation requires permission for the transport by the radiation protection authorities. Moreover, millimetric (or micrometric for solid state microdosimeters) sensitive volumes do not fit with the larger dimensions of these internal calibration sources. Alternative techniques, such as those based on the proton and/or the electron edge of the microdosimetric spectra (Bianchi et al., 2021) and the electronic calibration for silicon detectors are employed for this purpose. These techniques are discussed in the following section.

## 4. Detectors for assessing the quality of hadron therapy fields

### 4.1. Tissue-equivalent proportional counters

The reference detector for microdosimetry is the tissue-equivalent proportional counter (TEPC). For microdosimetry of hadron therapy beams, mini-TEPCs with a millimetric sensitive volume were designed and constructed at the INFN-Legnaro National Laboratories (De Nardo et al., 2004a). A sectional view of this detector is shown in Fig. 4.

Its external diameter (2.7 mm) is the same as that of an 8 french (i.e. 2.7 mm) cannula which is employed for mini-invasive surgery. The mini-TEPC sensitive volume is cylindrical (diameter and height 0.9 mm). The anode is a wire of gold-plated tungsten, 10 μm in diameter, and the cathode is made of Shonka A-150 plastic, 0.35 mm in thickness. The mini-TEPC is inserted in a titanium probe 2.7 mm in diameter, 170 mm in length, electrically grounded. The insulation between the conductive A-150 cathode and the titanium probe is ensured by a Rexolite cylinder 0.35 mm in wall thickness. The propane-based tissue-equivalent gas flows continuously through the sensitive volume in order to avoid aging effects that can give rise to gas gain shifts.

This mini-TEPC proved to be capable of operating in gas-steady modality for a few months (Conte et al., 2019), thus allowing the access to radiotherapy rooms where the use of flammable gases, such as propane, is prohibited. Measurements were performed at different positions across the Bragg peak of the CATANA facility. Subsequently, they were repeated at the same positions after four months for checking the mini-TEPC stability, showing a very satisfactory agreement (within 3%) with the microdosimetric spectra acquired previously.

The very small dimensions of this TEPC allowed to perform microdosimetric measurements and to assess the beam quality inside a phantom irradiated with protons for the eye tumour treatment at the Centre Antoine-Lacassagne (Nice, France) (De Nardo et al., 2010) and at the CATANA facility of the INFN-Laboratori Nazionali del Sud (Catania, Italy) (De Nardo et al., 2004b). In those works, the quality of the therapeutic beam was assessed in terms of $RBE_{\mu}$ (equation (11)), by using the *r(y)* weighting function by Loncol et al. (1994), which was calculated from both microdosimetric and radiobiological measurements in 14 different irradiation centres. The microdosimetric spectra (assessing the *y* dependence of the *r(y)* function) were measured in a 2 μm simulated site. More recently, several measurements were performed for assessing the radiation quality of hadron therapy facilities with the mini-TEPC (De Nardo et al., 2010; Colautti et al., 2018a, 2018b; Conte et al., 2019, 2020; Bianchi et al., 2020a, 2020b). These measurements were conducted both with therapeutic proton and carbon ion beams. In particular, Colautti et al. (2018) performed the first microdosimetric characterization of the CNAO carbon ion beam delivered with an active scanning system.

Another instrument devoted to radiation therapy applications is the twin miniaturized TEPC (Moro et al., 2006), which was developed for microdosimetry in boron neutron capture therapy (BNCT). It consists of a cylindrical container (diameter 2.7 mm, length 200 mm) housing two cylindrical TEPCs, 0.57 $mm^3$ in sensitive volume. The cylindrical TEPC cathodes are made of A-150 plastic, 0.35 mm in wall thickness. The wall of one TEPC is enriched in $^{10}B$. The anodes are gold-plated wires 10 μm in thickness. The TE propane-based gas continuously flows through the TEPCs to maintain the stability of its gain despite the high count-rate of the therapeutic field.

The calibration of the mini-TEPCs is carried out with the intrinsic proton and/or the electron edge technique. It should be remembered that the proton edge (p-edge) is the region of the microdosimetric spectrum which decreases sharply at high *y* values and which corresponds to the maximum energy imparted by protons to the sensitive volume. Similarly, the electron edge corresponds to the maximum energy imparted to the sensitive volume by secondary electrons generated by a gamma-ray source. This method can be used when the proton edge is not visible, i.e., when the radiation field is constituted mainly by low-LET radiation. While accelerated proton beams and neutron sources (i.e., recoil-protons from neutron elastic scattering) are necessary for the proton edge calibration, isotopic gamma-ray sources like $^{137}Cs$ and $^{60}Co$ can be used for the one based on the e-edge (Parisi et al., 2020).

Bianchi et al. (2020) studied the accuracy of two markers for determining the position of the p-edge from a $^{7}Li(p,n)$ neutron source and the 62 MeV proton beam at CATANA, after fitting the microdosimetric distribution at high *y* values with a Fermi-like function. The markers are the position of the inflection point $h_{flex}$ of the fitted p-edge in the pulse-height distribution *h* and the intercept $h_{tC}$ of the tangent to the inflection point with the pulse-height axis. $h_{flex}$ is less sensitive to undetected variations of the gas pressure and its uncertainty was found to be lower than 3%. The *y*-value corresponding to $h_{flex}$ was calculated with Monte Carlo simulations performed with the FLUKA (Ferrari et al., 2005; Bohlen et al., 2014) code. The maximum energy deposited by protons in the mini-TEPC turned out to be 97 keV, while a thorough discussion was made in that work about the mean chord length distribution. In the definition of the lineal energy, the mean chord length distribution $\overline{\ell}$ refers to a uniform isotropic random distribution of chords. However, except for sensitive volumes in shape of a sphere (where $\overline{\ell} = 2/3D$, where *D* is the diameter, and the path length distribution is independent of the irradiation geometry) and for the case of a right cylinder irradiated by parallel beams (as usually occurs for therapeutic charged hadron beams), the path length distribution generally differs from that of isotropic chords. In other words, for cylindrical (the mini-TEPC) or slab detectors (silicon detectors) the imparted energy distribution is more related to that of the path lengths rather than that of the geometrical chord lengths, at least for low-LET events. In such a situation, the lineal energy can be calculated as the ratio of the imparted energy to the mean value of the path length of the primary tracks intersecting the sensitive volume, which is more related to the LET (Bolst et al., 2017). However, it should be emphasized that this way of evaluating the lineal energy deviates from its ICRU definition. The application of this alternative procedure should be always explicitly stated. A method for converting the microdosimetric spectra from a slab to different geometries was discussed in details by Magrin (2018).

An avalanche-confinement TEPC operating at a nanometric level was designed and constructed by Cesari et al. (2002) and upgraded by Bortot et al. (2017a). The design of the new TEPC includes a thinner-walled chamber, which allows measuring low-energy (and high-LET) hadron beams, a removable internal alpha source and a very compact solid-state detector (SSD) inserted into the sensitive zone for energy calibration. The TEPC was designed for simulating sites in the range from 0.3 μm down to 25 nm.

The cylindrical sensitive volume of the detector (13 mm in diameter and length) houses three electrodes biased independently: a central

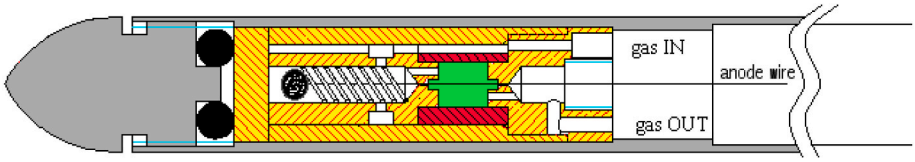


**Fig. 4.** A sectional view of the mini-TEPC designed and constructed at the INFN-Laboratori Nazionali di Legnaro (De Nardo et al., 2004a). Its millimetric sensitive volume is in green.

anode wire (graphite, 1 mm in diameter), a cylindrical cathode shell (conductive plastic A-150 type, 13 mm in internal diameter and 1 mm in thickness) and a helix (gold-plated tungsten, 100 μm in diameter) made of 19 coils, 6 mm in inner diameter. This helix surrounds the anode wire and subdivides the sensitive volume into an external drift zone and an internal multiplication region (Fig. 5).

Two field tubes (stainless steel, 6 mm in diameter) are employed both for sustaining the helix and for defining the sensitive volume, which is a right cylinder 13 mm both in diameter and length, thus avoiding any distortion of the electric field, while two insulating Rexolite caps enclose the chamber. An orifice was drilled into the basis cap to allow a gas flow. Two aligned holes were also drilled into the Rexolite caps in order to contain a thick removable Cm-244 alpha source, sealed by a mylar layer, and a miniaturized solid-state detector (SSD). This configuration allows calibrating the TEPC by also varying *i)* the simulated site size and *ii)* the polarization of the three electrodes. It guarantees that only signals due to alpha particles with a straight path inside the sensitive volume, i.e. the drift region, are collected (Bortot et al., 2017b). Particles ionizing the gas inside the multiplication region affect slightly the microdosimetric distribution, since its volume is about 20% of the whole sensitive region and charge multiplication of particles ionizing the gas inside the confining helix is lower. This avalanche-confinement TEPC showed to be capable of measuring in the range 0.3 μm–25 nm when irradiated with carbon (Bortot et al., 2017a), helium (Mazzucconi et al., 2019b) ions and protons down to 35 nm (Mazzucconi et al., 2019a). A characterization of 195.2 MeV per nucleon carbon ions irradiating a PMMA phantom was carried out at the CNAO by simulating site sizes in the range 25–500 nm (Bortot et al., 2020). The spectra turned out to be influenced by secondary delta-ray electrons when decreasing the site size for the same phantom depth. A shift towards high lineal energies was observed while decreasing the site size at depths proximal to the Bragg peak. At distal depths, the edge of the spectrum was found to be independent of the simulated site size. The same independence was also observed for helium ions, the CATANA clinical proton beam and when irradiating the detector with a $^{137}$Cs source.

It should be stressed that the geometry of the sensitive volume, defined by the hollow-cylindrical drift region external to the helix, together with the presence of the fairly thick central anode lead to calculate the mean chord length depending on the irradiation geometry (which is a parallel beam normal to the anode for charged hadron beams) with Monte Carlo simulations or analytically (Mazzucconi et al., 2018).

A further development of the avalanche-confinement TEPC described above consists in drilling a hole in the whole detector with a direction parallel to the anode axis (Mazzucconi et al., 2020a; 2020b). The detector was installed along the beam line of the STARTRACK nanodosimeter for directly comparing microdosimetric and nanodosimetric data. A Monte Carlo code was developed for simulating the electron avalanche process inside this detector (Mazzucconi et al., 2020c).

A millimetric multi-element TEPC based on a gas electron multiplier (GEM) has been developed by Ferrari et al., 2005), Ferrari et al., 2005, Ferrari et al., 2005, Ferrari et al., 2005. This device consists of five cylindrical cavities of 4.3 mm$^3$ in sensitive volume sandwiched between two layers of A-150 plastic and filled with a TE gas. Electrons from ion pair creation are drifted to the GEM, which provides charge multiplication. The microdosimetric response of a TEPC-GEM (five cylindrical sensitive volumes 18 mm in diameter and height, GEM hole diameter 60 μm, 90 μm pitch) to 14 MeV neutrons and a $^{252}$Cf source was measured by Ferrari et al., 2005) and an excellent agreement was found with spectra available in the literature.

A GEM microdosimeter consisting of 16 independent TEPCs over a 144 mm$^2$ area was designed and constructed by De Nardo et al. (2017). The GEM-TEPC consists of an A-150 plastic cathode, a 2 mm thick drift region filled with propane gas, a GEM foil and a read-out printed circuit board (PCB). The PCB consists of a large electrode and 16 pads 2 mm in diameter isolated by guard rings. This configuration provides 16 cylindrical sensitive volumes (inside the gas drift region) acting like 16 independent mini-TEPCs, which are read independently by the front electronics. Irradiations performed with a $^{137}$Cs gamma ray source and in a neutron field showed an excellent agreement with other TEPCs (De Nardo et al., 2017).

The use of a gas microstrip detector (GMD) for microdosimetry has been studied by Waker et al. (2009) and (Dubeau et al. (2000) . This instrument consists of alternating anode and cathode metallic strips lithographically printed on a substrate, a region housing the counting gas (propane-based TE gas) 650 μm in thickness and a drift electrode (made of A-150 TE plastic). The proportional gas multiplication occurs in the proximity of the anodes. The mean chord length of this device was 550 μm which corresponds to a simulated mean chord length of 0.36 μm in tissue at a gas pressure of 0.6 atm. The low yield of useable printed substrates and aging effects of GMDs brought to study an alternative configuration of a micro-patterned TEPC, by inserting a GEM above the read-out plane (Waker et al., 2009; Dubeau and Waker, 2008). The GEM decouples the avalanche and the read-out elements, thus allowing the design of read-out strips with more flexibility. The readout pattern consists of 128 strips 300 μm in width and 400 μm in pitch. Each readout strip samples a cuboid gas volume of 0.4 × 0.82 × 75 mm$^3$ which corresponds to a simulated mean chord length of 0.56 μm. The $H^*(10)$ response of this detector was shown to be improved for low energy reactor-like fields compared to that of a conventional TEPC and its sensitivity was about 75 counts per μSv. This could allow employing two stacked units of such a GEM-based TEPC for personal neutron dosimetry (Wroe et al., 2009; Dubeau and Waker, 2008).

More recently, a new configuration of a TEPC based on a thick gas

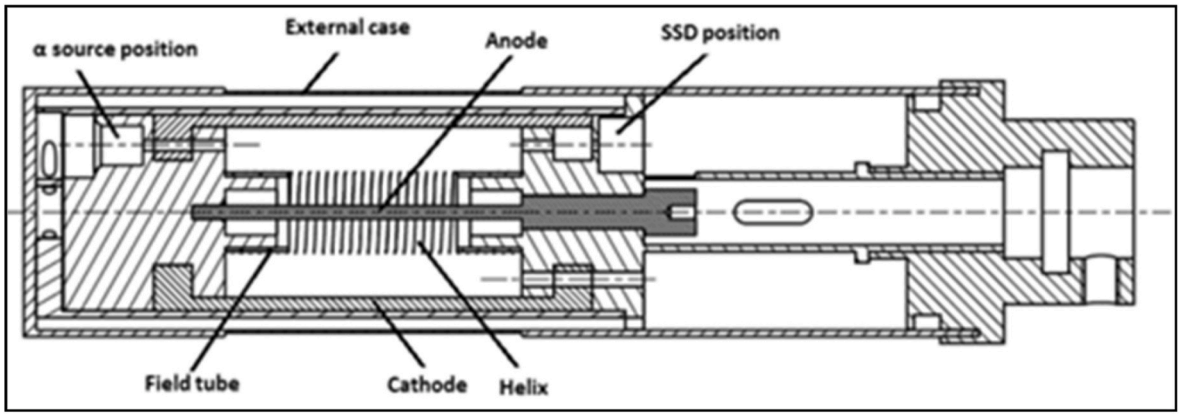


**Fig. 5.** Cross-sectional view of the avalanche-confinement TEPC. The locations of the calibration alpha source and the solid state detector (SSD) are indicated.

electron multiplier (THGEM) has been proposed by (Byun et al., 2009). The THGEM thickness ranges from sub millimetric to millimetric order (while the standard GEM insulator foil is about 50 μm in thickness) and also the diameter of the holes is also larger, allowing the holes to be machined by drilling (a dedicated and more expansive process is required to manufacture the holes of standard GEMs). Thus, the THGEM is more robust and practical for gas amplification in a two-dimensional microdosimeter (Byun et al., 2009). Byun et al. (2009) simulated the variation of the electric field along the hole axis of THGEMs of different thickness and hole diameter, together with the electron avalanche. Preliminary tests were performed using a cylindrical TEPC (5 mm in diameter and 5 mm in height) coupled to a THGEM prototype (0.1 mm in thickness, hole diameter 0.35 mm). The prototype was irradiated with a mixed neutron-photon field generated by bombarding a thick LiF target with 2.3 MeV protons. The results are very promising: the acquired spectra showed the expected distributions due to neutrons and photons. The distribution of low-LET events (mainly electrons from photon interactions) was partially obscured by the electronic noise, thus requiring an increase of the avalanche gain.

### 4.2. Silicon microdosimeters

The micrometric sensitive volumes (SV) which can be fabricated for silicon detectors have led to these devices being studied as microdosimeters. They can be applied for assessing single event effects in electronic instrumentation exposed to complex fields around high-energy accelerators or in space missions. When coupled to tissue-equivalent converters or inserted in tissue-equivalent phantoms, they can be used for measuring the quality of radiation therapy beams. Detailed reviews of silicon microdosimetry were given by Bradley et al. (2001), Agosteo and Pola (2011) and Rosenfeld (2016). The use of micrometric volumes avoids the contribution of wall effects (ICRU, 1983) to the measured spectra. The wall effect refers to events depositing their energy in the TEPC sensitive volume (such as a pair of charged particles created in the TEPC walls), which would be acquired partially in a micrometric site of tissue (e.g. only a single charged particle of the pair mentioned above hits the micrometric volume for geometrical reasons). Further advantages of such a detector are its compactness, transportability, low power consumption and a low sensitivity to vibrations. However, the following problems must be solved when using a silicon device for microdosimetry: i) the sensitive volume has to be confined in a region of well-known dimensions. In a silicon detector, the sensitive volume may depend on the particle LET because of the field-funnelling effect. This effect causes a local distortion of the electric field in the sensitive zone, induced by high-LET particles, which leads to charge collection outside the depleted region. Moreover, charge diffusion outside the sensitive volume and charge collection from the lateral SV outer zone can contribute to increase its effective dimensions; ii) the electric noise limits the minimum detectable energy. This is due to the high-capacitance (up to a few nF) of a very thin sensitive zone; iii) corrections for tissue-equivalence must be made for the silicon sensitive zone; iv) correction for shape equivalence must be made when referring to a site with a different geometry, since the sensitive zone of a silicon device can be approximated by a cuboid; v) the angular response must be evaluated carefully; vi) the efficiency of a single detector of micrometric dimensions is very poor and detector arrays should be considered.

Moreover, the slope of the proton edge (and of the higher lineal energy edges referring to heavier ions, such as helium, carbon etc.) can be sharper especially for silicon detectors showing thick (e.g., 10 μm) sensitive volumes, when compared to that of a TEPC simulating a micrometric site size. It should be remembered that the range of the highest-LET protons is about 1 μm in water, while the minimum thickness of the available silicon devices is 2 μm, which corresponds to 3.3 μm in water (considering 2.3 g $cm^{-3}$ as the silicon density and 0.75 as the average mass stopping power ratio to water). Therefore, protons with the higher LET tend to stop completely at silicon depths shorter than the SV thickness thus depositing all their energy and hiding effects of partial energy deposition due to the energy straggling. It should be mentioned that the smoother decrease of the proton edge in a TEPC is also due to the statistics of the avalanche multiplication close to its anode. When the proton edge is predominant, this difference in slope can also influence the $\bar{y}_D$ value. On the other hand, the thicker is the SV of a silicon detector (with the same sensitive area), the lower is its capacitance and therefore its minimum detectable lineal energy. Therefore, thicker (e.g., 10 μm, corresponding to about 17.2 μm in water) silicon microdosimeters (showing a lineal energy threshold of the order of 1 keV $\mu m^{-1}$) should be used in the proximal part of the proton Bragg peak (where the LET is lower), while the thinner (e.g., 2 μm, corresponding to about 3.3 μm in water) ones should be used in its distal fall-off (where the LET is higher). Usually, this does not hold for therapeutic carbon ions, since their LET values are higher at all depths across their Bragg peak and therefore thin silicon SVs can be employed with minor limitations.

It should be stressed that the ΔE stage of the silicon telescope (the one acting as a microdosimeter) is too thin for calibrating it with a source of alpha particles stopping completely in it. Therefore, the proton edge can be exploited for this purpose either through irradiations with proton beams from an accelerator or recoil-protons from a neutron source (by coupling the detector with a recoil proton converter). In any case, these procedures do not provide any information about the linearity of the device. An alternative way is to perform the electronic calibration summarized in the following.

Generally, a silicon detector can be modeled as a capacitor: a sharp variation of the polarization voltage occurs at the terminals of this capacitor when a charged particle is detected. This phenomenon can be reproduced through a test input constituted by a test capacitor ($C_{test}$) connected directly to the electrode collecting the charge. In this way, a current pulse $i(t)$, equal to that induced by the radiation-detector interaction, can be generated by applying a step signal $V_{test}(t)$ with an optimized amplitude. In other words, an amount of charge $Q_{inj}$, equal to that generated in the silicon detector by the interacting particle, is injected into the preamplifier input. It should be stressed that this holds only if the value of the test capacitance $C_{test}$ is known accurately.

The assessment of the test capacitance $C_{test}$ applied to the preamplifier input is carried out by connecting a thick silicon detector (with a junction capacitance negligible with respect to that of ΔE stage) to the electronic chain of the ΔE stage. Then the thick device is irradiated with a $^{137}Cs$ calibration source (as an example) and the spectrum of its conversion electrons is acquired. A test signal $V_{test}(t)$ is then applied to $C_{test}$ for generating a peak centered at the same channel where the 624 keV conversion electron peak is measured. In such a way, the charge $Q_{inj}$, injected through the capacitor $C_{test}$, is equivalent to the charge $Q_{ec}$ generated in a thick silicon detector by the 624 keV conversion electrons:

$$C_{test} = \frac{E_{peak}}{V_{test}} \frac{q}{\varepsilon_{Si}} \tag{15}$$

where $E_{peak}$ is the energy corresponding to the considered peak (624.2 keV in this case), $\varepsilon_{Si}$ is the average energy required to generate an electron-hole pair in silicon, $\varepsilon_{Si} = 3.62$ eV/pair (Knoll, 2010) and $q$ the charge of a single electron ($q \approx 1.6 \times 10^{-19}$ C).

Since $C_{test}$ is known, a series of test signals $V_{test}$ of a different amplitude can be injected for obtaining a series of peaks in the MCA spectrum which simulate the ones referring to an actual detector irradiation with mono-energetic particles of different energies.

*Thus, the calibration curve can be obtained by fitting the energy-channel data from test signals of different amplitudes. The linearity of the detection system can also be assessed.*

A very detailed and comprehensive review of the silicon microdosimeters designed by the Centre for Medical Radiation Physics (CMRP, Wollongong, Australia) was given by Rosenfeld (2016). The first

device was described by Bradley et al. (2001) and Prokopovich et al. (2008). It consists of an array of diodes fabricated by using the silicon on insulator (SOI) technology. This technique allows sensitive volumes of well-defined dimensions to be obtained, independent of the field funnelling effect. Different structures with a sensitive volume 2, 5 and 10 μm in thickness were fabricated. The first planar 2D geometry was based on an array of cuboids of 30 × 30 $\mu m^2$ base area. The absorbed dose distributions from different neutron fields were compared to simulations performed with the GEANT code (Agostinelli, 2003; Allison, 2006) and measurements with a standard TEPC, resulting in a satisfactory agreement.

Irradiations with an alpha-particle microbeam showed that the charge collection efficiency of this first-generation device was dependent on the position of interaction inside the sensitive volume because of the radial distribution of the electric field and charge diffusion. In any case, the size of the sensitive volume (SV) could be adjusted with pulse-shape analysis and the device was employed successfully in many applications, such as in proton therapy. A second generation microdosimeter with an array of 2500 cylindrical sensitive volumes 2, 5 and 10 μm in thickness was fabricated on a SOI layer. A guard ring was provided for hindering charge collection outside the SVs. The third generation microdosimeter consisted of a planar array of cylindrical SVs 6 and 10 μm in diameter on a 10 μm thick high-resistivity SOI substrate. The acquisition of events outside the SV was hindered by a veto p + electrode.

The fourth generation microdosimeter consists of freestanding-on-silicon oxide 3D SVs, which showed to prevent charge sharing and charge collection outside the SV. In other words, the freestanding 3D SV was obtained by removing the adjacent silicon structure (thus making impossible any lateral charge diffusion), through the "mesa" technology. This "bridge microdosimeter" consists of an array of 4248 cuboid SVs 30 × 30 $\mu m^2$ in sensitive area and 10 μm in thickness. The etching technique used for fabricating this array generates the cuboid SVs leaving a thin silicon bridge between them for supporting the aluminium tracks (Rosenfeld, 2016).

The fifth configuration proposed by CMRP ("mushroom" SOI microdosimeter) consist of cylindrical SVs 10 μm in diameter and thickness embedded in polymethylmethacrylate (PMMA) tissue-equivalent layer.

3D silicon microdosimeters for hadron therapy applications were also designed and constructed by Guardiola et al. (2020). The first proposed device consists of 3D columnar SVs inserted between p-n junctions fabricated on SOI wafers (ultra-thin-3D-diodes, U3DTHIN). A square array of columnar electrodes was fabricated and the SVs were 10 and 20 μm in thickness. The second configuration was based on an array of cylindrical SVs with diameters from 9 to 25 μm and 5, 10 and 20 μm in thickness again fabricated on SOI wafers. The U3DTHIN microdosimeter was irradiated with 62 MeV protons at the Center de Recherche du Cyclotron (Louvain-La-Neuve, Belgium) and with 94.96 MeV per nucleon carbon ions at Grand Accélérateur National d'Ions Lourds (GANIL, France), showing a good agreement with simulated data. Some limitations due to their dynamical range and pile-up were observed for the carbon ion irradiations. The 3D cylindrical array was irradiated with 115.23 MeV per nucleon carbon ions at CNAO. An excellent agreement was found between experimental and simulated $\bar{y}_D$ values.

A monolithic silicon telescope was proposed by Agosteo et al. (2006) as a microdosimeter, basing on a detector designed by Tudisco et al. (1996) and fabricated by ST Microelectronics (Catania, Italy). The first model consisted by a single ΔE element 2 μm in thickness and a 500 μm thick residual energy E-stage. The ΔE and the E elements are separated by a deep-implanted p + electrode which acts a watershed for charge collection, thus minimizing the field-funnelling effect. The thin ΔE element acts as a microdosimeter. The SV sensitive area is about 1 $mm^2$. This single-stage configuration showed some limitations for an isotropic irradiation field since the length of a tilted particle track can be millimetric. In any case, this microdosimeter showed a good agreement with a mini-TEPC (Section 4.1) when irradiated with parallel clinical beams.

The pixelated silicon microdosimeter proposed by Agosteo et al. (2008) minimizes the effect mentioned above. It consists of a matrix of cylindrical ΔE elements (about 2 μm in thickness) and a single residual-energy E stage (500 μm thick). The nominal diameter of the ΔE elements is about 9 μm and the width of the pitch separating the elements is about 41 μm. More than 7000 pixels are connected in parallel to give an effective sensitive area of about 0.5 $mm^2$. A guard ring hinders charge collection outside the SV. The minimum detectable energy is limited to about 20 keV (corresponding to about 7–8 keV $\mu m^{-1}$ in lineal energy) by the electronic noise. Therefore, the applicability of this silicon microdosimeter is limited to high LET particles. The ΔE stage acts as a microdosimeter and the E stage plays a fundamental role for assessing the full energy of the interacting particles, thus allowing an LET-dependent correction for tissue-equivalence to be performed event-by-event. An example referring to proton irradiations is given in the following.

The event-by-event tissue-equivalence correction can be adopted when protons stop completely in the E stage, thus allowing to measure their impinging energy. This complete energy deposition in the silicon telescope occurs for protons up to about 10 MeV, whose range in silicon corresponds to the thickness of the E-stage (500 μm). In the energy range below 10 MeV the ratio $R(E_p)$ of the stopping power of protons in tissue $S^{Tissue}(E_p)$ to that in silicon $S^{Si}(E_p)$ shows a fairly high variation. In this case, the energy $E^{Si}_{\Delta E}$ (energy deposited in the silicon ΔE stage) can be corrected for the energy-dependent ratio $R(E_p)$:

$$E^{Tissue}_{\Delta E}(E_p) = E^{Si}_{\Delta E}(E_p) \cdot \frac{S^{Tissue}(E_p)}{S^{Si}(E_p)} \tag{16}$$

where $E_p$ is calculated by summing the energy deposited in both detector stages and $E^{Tissue}_{\Delta E}(E_p)$ is the corresponding energy which would be deposited in tissue.

When protons cross completely the E stage (i.e., above about 10 MeV), no information about the energy $E_p$ of the impinging protons is available. For these energies, the ratio $R(E_p)$ ranges from 0.556 to 0.585 and the use of an average factor $\zeta$ is acceptable. Therefore, the energy $E^{Si}_{\Delta E}$, measured with the silicon ΔE stage, is scaled with a constant factor $\zeta$ equal to 0.574, obtained by averaging over the energy interval of interest the energy-dependent ratio $R(E_p)$.

When comparing the microdosimetric spectra from a detector with a sensitive volume with a different geometry (e.g., a TEPC) a shape-equivalence correction have to be carried out. As described in details by Agosteo et al. (2008) for the silicon telescope described herein, this shape-equivalence correction consists in calculating the lineal energy $y$ by dividing the imparted energy $E^{Tissue}_{\Delta E}$ by an equivalent mean chord length $\ell_{eq}$, equal to the product of the actual mean chord length $\ell$ times a coefficient η (equal to 0.533). This coefficient was derived through parametric criteria discussed by Kellerer (1981). The coefficient η depends only on the geometry of the sensitive volume of the two detectors.

For heavy ion beams in radiotherapy, Bolst et al. (2017) demonstrated that the adoption of the mean path length of particles traversing the SV instead of the mean chord length allows assessing more accurate $RBE_\mu$ values. The mean path length can be approximated by the SV thickness when irradiating SOI microdosimeters with slab SVs. This assumption does not hold for lighter charged hadrons, such as protons, since Coulomb nuclear scattering cannot be neglected.

The microdosimetric spectra acquired at the CATANA facility at four position across the distal fall-off of the 62 MeV proton Bragg peak is shown in Fig. 6 (Agosteo et al., 2010).

The $d(y)$ distribution measured with a cylindrical TEPC under the same irradiation conditions is shown in the figure. The $d(y)$ spectrum of the silicon microdosimeter was derived after correcting for tissue equivalence and for the different shape of the particle track distribution inside the two cylindrical sites (ΔE element and TEPC) of different dimensions, thus referring to the same site size.

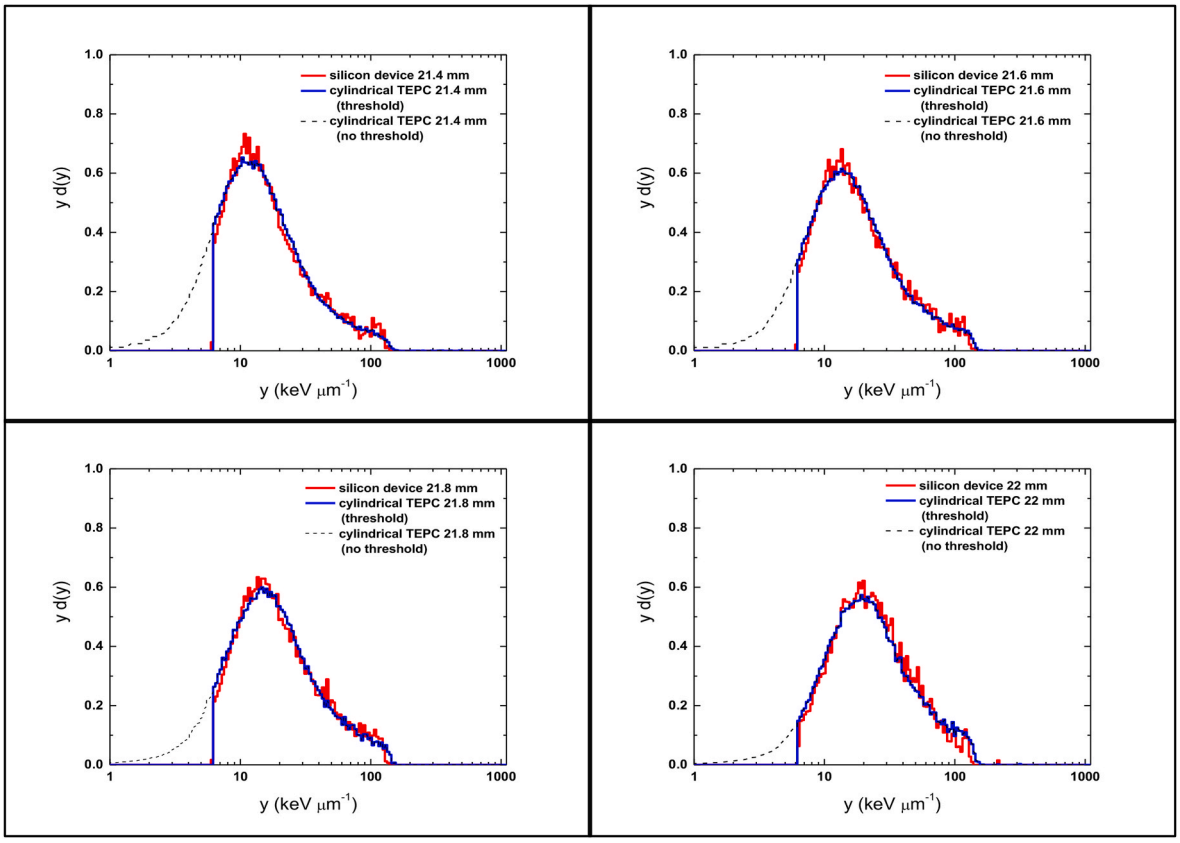


**Fig. 6.** Comparison between the lineal energy spectra obtained with the silicon telescope (red line) and those obtained with the reference TEPC (solid blue line) truncated at a value corresponding to the energy threshold of the silicon-based system (6 keV $\mu m^{-1}$). The non-normalized complete microdosimetric spectra measured by the TEPC are also shown (dashed blue line).

The microdosimetric spectrum derived by applying the constant correction factor ζ instead of the event-by-event procedure is shown in Fig. 7 together with that measured by the TEPC at a depth of 22 mm (to be also compared with Fig. 6d). The adoption of a constant correction factor leads to a shift of the spectrum towards lower *y*-values, together with an overestimate of the peak at about 10 keV $\mu m^{-1}$.

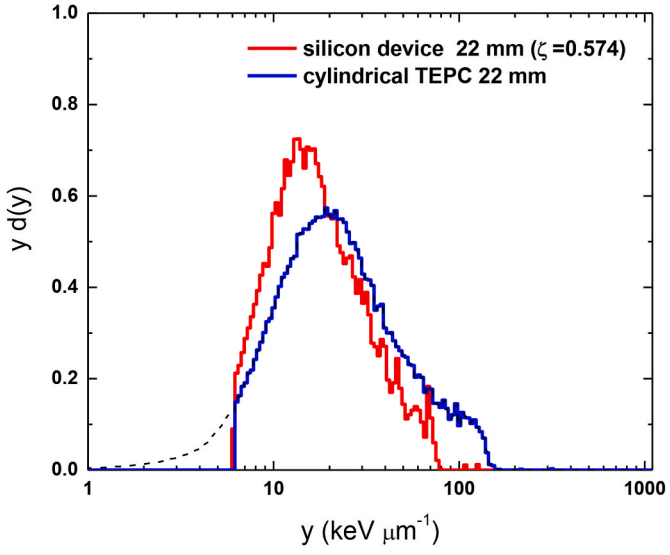


**Fig. 7.** Comparison between the lineal energy distribution obtained with the silicon telescope by applying the constant correction factor $\zeta = 0.574$ and that measured with the TEPC at the same depth (Fig. 6, right bottom).

The response of this pixelated telescope detector to a therapeutic proton beam is discussed by Agosteo et al. (2010). Irradiations with the scanning-active beam of carbon ions at the CNAO (Colautti et al., 2018b) showed some differences at low y-values of the microdosimetric spectra measured with the pixelated silicon microdosimeter and a mini-TEPC (Section 4.2). However, at various depths across the Bragg peak, these differences did not influence the relative absorbed dose and the $\bar{y}_D$ corrected for the saturation effect.

### 4.3. *Diamond microdosimeters*

Diamond is an alternative material which is being studied as a solid state microdosimeter, showing a better tissue-equivalence than silicon. Sensitive volumes of dimensions down to a few microns can be fabricated with different techniques. The average energy required to generate an electron-hole pair in diamond is $\varepsilon_D = 12.8$ eV (Zahradnik et al., 2020), leading to a lower energy resolution when compared to silicon detectors $\varepsilon_{Si} = 3.62$ eV/pair (Knoll, 2010).

Verona et al. (2018) designed and constructed a CVD diamond-based microdosimeter 0.3 × 0.3 $mm^2$ in sensitive area and 2 μm in thickness, corresponding to 6.1 μm in water, considering 3.5 g $cm^{-3}$ in density and an average mass stopping power ratio of 0.87 (Colautti et al., 2018a). The microwave plasma enhanced CVD (chemical vapour deposition) technique for its fabrication was described in details by Ciancaglioni et al. (2011). The detector is based on a p-i-metal structure and the metallic rectifying contact shows a Schottky barrier of about 1.2 eV. This allows to avoid applying an external supply voltage.

Its application for assessing the quality of carbon ion beams is discussed by Colautti et al. (2018). For those measurements the detector was calibrated through the carbon edge and its minimum detectable energy was about 10 keV $\mu m^{-1}$, thus requiring the linear extrapolation

down to 0.01 keV $\mu m^{-1}$ of the frequency spectrum.

An array of 4 × 4 micro-SVs, each one 60 μm in diameter and 8 μm in thickness was fabricated by Zahradnik et al. (2020) with the single crystal CVD technique. Even in this case, the p + -i junction provides self-biasing. A guard ring surrounds each cylindrical SV in order to prevent charge diffusion. The detector was characterized with a 2 MeV proton microbeam, showing to be promising for assessing the quality in proton therapy fields.

A detailed review of the available fabrication techniques of diamond detectors and their capabilities of satisfying the requirements for their application in microdosimetry is given by Davis et al. (2019).

### 4.4. Detector comparison

Colautti et al. (2018a) compared the response of four detectors (a mini-TEPC, a silicon telescope, a GEM and a diamond microdosimeter) irradiated with a beam of 62 MeV per nucleon carbon ions at the INFN-LNS in Catania (Italy). The acquired microdosimetric spectra showed significantly different shapes, as expected, since the detector SVs were different together with the properties of their constituting materials. Nevertheless, a better agreement was found for the $\bar{y}_D$ values at the measured depths across the Bragg peak in a PMMA phantom. A similar trend was observed in (Colautti et al., 2018b), where the response of a mini-TEPC and a silicon telescope microdosimeter were compared for the therapeutic active scanning beam at the CNAO.

Bianchi et al. (2020a) compared the microdosimeric spectra from the mini-TEPC and a silicon telescope at various depths across the Bragg peak from the 62 MeV proton beam at the INFN-LNS CATANA facility. Again, the shape of the spectra showed some deviations even after the linear extrapolation of the silicon detector spectra down to 0.01 keV $\mu m^{-1}$. These discrepancies were attributed to the different chord length distribution and to the presence of wall effects in the mini-TEPC. In particular, the lineal energy distribution was found to be wider especially at low y-values. This was due to a higher contribution of δ-rays from the TEPC wall. In this case, the different shape of the microdosimetric spectra led to overestimate the $\bar{y}_D$ values from the silicon device. However, the trend of the $\bar{y}_D$ values against the depth of the Bragg peak was in a satisfactory agreement with the TEPC one. Therefore, a scaling factor was applied, resulting in a sort of a $\bar{y}_D$ -calibration of the silicon microdosimeter.

## 5. Conclusions

Different detectors are being studied for assessing the quality of hadron therapy fields. TEPCs can be considered the reference instrumentation for microdosimetry, since they can measure a wide range in lineal energy (from tenths to several thousands of keV $\mu m^{-1}$), being based on gas electron multiplication. Moreover, their sensitive volume is well defined and does not suffer from charge collection and diffusion like in silicon devices. Therefore, when characterizing a new device (e.g., silicon or diamond microdosimeters), its response should be compared with the one from a standard TEPC.

The high capacitance of the thinnest silicon SVs (about 2 μm) limits their use in low LET beams (e.g., in the proximal part of the Bragg peak from therapeutic protons), since the related signals cannot be distinguished from the electronic noise. Therefore, devices with a thicker SV (about 10 μm) can be used at shallow depths, since the most of the low LET particles are crossers and the microdosimetric spectrum is less influenced by stoppers, which would be crossers in a TEPC simulating a micrometric site. Thinner SVs can be applied with minor concern to carbon ion beams.

All solid-state devices must be corrected for tissue-equivalence and, when comparing their spectra with the one from a TEPC of a different geometry, for shape-equivalence.

The first intercomparisons seem to give promising results in the use of different devices for assessing the quality of hadron therapy fields. In any case, the response of new devices should be compared with the one of a reference TEPC in different irradiation conditions.

## Declaration of competing interest

The authors declare that they have no known competing financial interests or personal relationships that could have appeared to influence the work reported in this paper.

## References


Agosteo, S., Colautti, P., Fazzi, A., Moro, D., Pola, A., 2006. A solid state microdosimeter based on a monolithic silicon telescope. Radiat. Protect. Dosim. 122, 382–386.

Agosteo, S., Fallica, P.G., Fazzi, A., Introini, M.V., Pola, A., Valvo, G., 2008. A pixelated silicon telescope for solid state microdosimetry. Radiat. Meas. 43, 585–589.

Agosteo, S., Cirrone, G.A.P., Colautti, P., Cuttone, G., D'Angelo, G., Fazzi, A., Introini, M. V., Moro, D., Pola, A., Varoli, V., 2010. Study of a silicon telescope for solid state microdosimetry: preliminary measurements at the therapeutic proton beam line of CATANA. Radiat. Meas. 45, 1284–1289.

Agosteo, S., Cirrone, G.A.P., D'Angelo, G., Fazzi, A., Introini, M.V., Pola, A., 2011. Feasibility study of radiation quality assessment with a monolithic silicon telescope: irradiations with 62 AMeV carbon ions at LNS-INFN. Radiat. Meas. 46, 1534–1538.

Agosteo, S., Pola, A., 2011. Silicon microdosimetry. Radiat. Protect. Dosim. 143, 409–415. https://doi.org/10.1093/rpd/ncq408.

Agostinelli, S., et al., 2003. GEANT4 – a simulation toolkit. Nucl. Instrum. Methods A506, 250–303.

Allison, J., et al., 2006. GEANT4 developments and applications. IEEE Trans. Nucl. Sci. 53, 270–278.

Bianchi, A., Colautti, P., Conte, V., Selva, A., Agosteo, S., Bortot, D., Mazzucconi, D., Pola, A., Reniers, B., Parisi, A., Struelens, L., Vanhavere, F., Tran, L., Rosenfeld, A.B., Cirrone, G.A.P., Petringa, G., 2020b. Microdosimetry at the 62 MeV Proton Beam of CATANA: preliminary comparison of three detectors. J. Phys. Conf. 1662, 012006.

Bianchi, A., Selva, A., Colautti, P., Bortot, D., Mazzucconi, D., Pola, A., Agosteo, S., Petringa, G., Cirrone, G.A.P., Reniers, B., Parisi, A., Struelens, L., Vanhavere, F., Conte, V., 2020a. Microdosimetry with a sealed mini-TEPC and a silicon telescope at a clinical proton SOBP of CATANA. Radiat. Phys. Chem. 171, 108730.

Bianchi, A., Mazzucconi, D., Selva, A., Colautti, P., Parisi, A., Vanhavere, F., Reniers, B., Conte, V., 2021. Lineal energy calibration of a mini-TEPC via the proton-edge technique. Radiat. Meas. 141, 106526.

Bohlen, T.T., Cerutti, F., Chin, M.P.W., Fassò, A., Ferrari, A., Ortega, P.G., Mairani, A., Sala, P.R., Smirnov, G., Vlachoudis, V., 2014. The FLUKA code: developments and challenges for high energy and medical applications. Nucl. Data Sheets 120, 211–214.

Bolst, D., Guatelli, S., Tran, L.T., Chartier, L., Lerch, M.L.F., Matsufuji, N., Rosenfeld, A. B., 2017. Correction factors to convert microdosimetry measurements in silicon to tissue in $^{12}C$ ion therapy. Phys. Med. Biol. 62, 2055–2069.

Bortot, D., Pola, A., Agosteo, S., Pasquato, S., Mazzucconi, D., Fazzi, A., Colautti, P., Conte, V., 2017a. A novel avalanche-confinement TEPC for microdosimetry at nanometric level. Radiat. Meas. 103, 1–12.

Bortot, D., Pola, A., Agosteo, S., Pasquato, S., Introini, M.V., Colautti, P., Conte, V., 2017b. A miniaturized alpha spectrometer for the calibration of an avalanche-confinement TEPC. Radiat. Meas. 106, 531–537.

Bortot, D., Mazzucconi, D., Pola, A., Fazzi, A., Pullia, M., Savazzi, S., Colautti, P., Conte, V., Agosteo, S., 2020. A nano-microdosimetric characterization of a therapeutic carbon ion beam at CNAO. Radiat. Phys. Chem. 170, 108674 https://doi.org/10.1016/j.radphyschem.2019.1086742-s2.0-85077454155.

Bradley, P.D., Rosenfeld, A.B., Zaider, M., 2001. Solid state microdosimetry. Nucl. Instrum. Methods B184, 135–157.

Byun, S.H., Spirou, G.M., Hanu, A., Prestwitch, W.V., Waker, A.J., 2009. Simulation and first test of a microdosimetric detector based on a thick gas electron multiplier. IEEE Trans. Nucl. Sci. 56, 1108–1113.

Cesari, V., Colautti, P., Magrin, G., De Nardo, L., Baek, W.Y., Grosswendt, B., Alkaa, A., Khamphan, C., Ségur, P., Tornielli, G., 2002. Nanodosimetric measurements with an avalanche confinement TEPC. Radiat. Protect. Dosim. 99, 337–342.

Chen, Y., Li, J., Li, C., Qiu, R., Wu, Z., 2018. A modified microdosimetric kinetic model for relative biological effectiveness calculation. Phys. Med. Biol. 63, 015008.

Ciancaglioni, I., Di Venanzio, C., Marinelli, M., Milani, E., Prestopino, G., Verona, C., Verona Rinati, G., Angelone, M., Pillon, M., Tartoni, N., 2011. Influence of the metallic contact in extreme-ultraviolet and soft x-ray diamond based Schottky photodiodes. J. Appl. Phys. 110, 054513.

Colautti, P., Conte, V., Selva, A., Chiriotti, S., Pola, A., Bortot, D., Fazzi, A., Agosteo, S., Treccani, M., De Nardo, L., Verona, C., Verona Rinati, G., Magrin, G., Cirrone, G.A. P., Romano, F., 2018a. Miniaturized microdosimeters as LET monitors: first comparison of calculated and experimental data performed at the 62 MeV/u 12C beam of INFN-LNS with four different detectors. Phys. Med. 52, 113–121.

Colautti, P., Conte, V., Selva, A., Chiriotti, S., Pola, A., Bortot, D., Fazzi, A., Agosteo, S., Ciocca, M., 2018b. Microdosimetric study at the CNAO active-scanning carbon-ion beam. Radiat. Protect. Dosim. 180, 157–161.

Colautti, P., Bianchi, A., Selva, A., Bortot, D., Mazzucconi, D., Pola, A., Agosteo, S., Petringa, G., Cirrone, G.A.P., Conte, V., 2020a. Therapeutic proton beams: LET, RBE and microdosimetric spectra with gas and silicon detectors. Radiat. Mesaurements. 136, 106386.

Colautti, P., Magrin, G., Palmans, H., Cortés-Giraldo, M.A., Conte, V., 2020b. Characterizing radiation effectiveness in ion-beam therapy Part II: microdosimetric detectors. Front. Physiol. 8, 550458 https://doi.org/10.3389/fphy.2020.550458.
Conte, V., Moro, D., Colautti, P., Grosswendt, B., 2015. Nanodosimetric descriptors of the radiation quality of carbon ions. Radiat. Protect. Dosim. 166, 214–218.
Conte, V., Bianchi, A., Selva, A., Petringa, G., Cirrone, G.A.P., Parisi, A., Vanhavere, F., Colautti, P., 2019. Microdosimetry at the CATANA 62 MeV proton beam with a sealed miniaturized TEPC. Phys. Med. 64, 114–122.
Conte, V., Agosteo, S., Bianchi, A., Bolst, D., Bortot, D., Catalano, R., Cirrone, G.A.P., Colautti, P., Cuttone, G., Guatelli, S., James, B., Mazzucconi, D., Rosenfeld, A.B., Selva, A., Tran, L., Petringa, G., 2020. Microdosimetry of a therapeutic proton beam with a mini-TEPC and a MicroPlus-Bridge detector for RBE assessment. Phys. Med. Biol. 65 (24), 245018.
Davis, J.A., Petasecca, M., Guatelli, S., Lerch, M.L.F., Rosenfeld, A.B., 2019. Evolution of diamond based microdosimetry. IOP Conf. Series: J. Phys. Conf. 1154, 012007 https://doi.org/10.1088/1742-6596/1154/1/012007.
De Nardo, L., Alkaa, A., Khamphan, C., Conte, V., Colautti, P., Ségur, P., Tornielli, G., 2002. A detector for track-nanodosimetry. Nucl. Instrum. Methods A 484, 312–326.
De Nardo, L., Cesari, V., Donà, G., Colautti, P., Conte, V., Tornielli, G., 2004a. Mini TEPCs for proton therapy. Radiat. Protect. Dosim. 108, 345–352.
De Nardo, L., Moro, D., Colautti, P., Conte, V., Tornielli, G., Cuttone, G., 2004b. Microdosimetric investigation at the therapeutic proton beam facility of CATANA. Radiat. Protect. Dosim. 110, 681–686.
De Nardo, L., Seravalli, E., Rosi, G., Esposito, J., Colautti, P., Conte, V., Tornielli, G., 2004c. BNCT microdosimetry at the TAPIRO reactor thermal column. Radiat. Protect. Dosim. 110, 579–586.
De Nardo, L., Colautti, P., Hérault, J., Conte, V., Moro, D., 2010. Microdosimetric characterisation of a therapeutic proton beam used for conjunctival melanoma treatments. Radiat. Meas. 45, 1387–1390.
De Nardo, L., Dal Corso, F., Pegoraro, M., 2017. Microdosimetric measurements in gamma and neutron fields with a tissue equivalent proportional counter based on a gas electron multiplier. Radiat. Protect. Dosim. 175, 260–266.
Dubeau, J, Waker, A.J., 2008. Neutron microdosimetric response of a gas electron multiplier. Radiat. Protect. Dosim. 128, 413–420.
Dubeau, J., Waker, A.J., Biggar, M., Rayner, M.D., Welch, E.W., 2000. Response to gamma rays and neutrons of a tissue-equivalent microstrip gas counter. Radiat. Prot. Dosim. 91, 391–401.
Ferrari, A., Sala, P.R., Fassò, A., Ranft, J., 2005. FLUKA: a Multi-Particle Transport Code. CERN 2005-10, INFN/TC_05/11, SLAC-R-773.
Grosso, M.F., Gagetti, L., Suarez Anzorena, M., Canepa, N., Real, N., Gun, M., Tacca, H., 2016. Present status of accelerator-based BNCT. Rep. Practical Oncol. Radiother. 21, 95–101.
Grosswendt, B., Conte, V., Colautti, P., 2014. An upgraded track structure model: experimental validation. Radiat. Protect. Dosim. 161 (1–4), 464–468.
Guardiola, C., Fleta, C., Quirion, D., Pellegrini, G., Gómez, F., 2020. Silicon 3D microdetectors for microdosimetry in hadron therapy. Micromachines 1 (12), 1053. https://doi.org/10.3390/mi11121053.
Gueulette, J., Octave-Prignot, M., De Costera, B.-M., Wambersie, A., Grégoire, V., 2004. Intestinal crypt regeneration in mice: a biological system for quality assurance in non-conventional radiation therapy. Radiother. Oncol. 73, S148–S154.
Gueulette, J., Liu, H.M., Jiang, S.H., Hsueh, J.H., De Coster, B.M., Liu, Y.H., Tsai, W.C., Wambersie, A., Chen, A.Y., 2006. Radiobiological Characterization of the epithermal neutron beam produced at the Tsing Hua open-pool reactor (THOR) for BNCT: comparison with other BNCT facilities. Therapeut. Radiol. Oncol. 13, 135–146.
Hawkins, R.B., 1996. A microdosimetric-kinetic model of cell death from exposure to ionizing radiation of any LET, with experimental and clinical applications. Int. J. Radiat. Biol. 69, 739–755.
Hawkins, R.B., 1998. A microdosimetric-kinetic theory of the dependence of the RBE for cell death on LET. Med. Phys. 25, 1157–1170.
Hsu, W-H., Braby, L.A., Reece, W.D., 2008. Detection system built from commercial integrated circuits for real-time measurement of radiation dose and quality using the variance method. Radiat. Protect. Dosim. 128, 5–11.
ICRU, 1983. International Commission on Radiation Units and Measurements. In: Microdosimetry. ICRU Report, vol. 36. ICRU, Bethesda, Maryland.
Kase, Y., Kanai, T., Matsumoto, Y., Furusawa, Y., Okamoto, H., Asaba, T., Sakama, M., Shinoda, H., 2006. Microdosimetric measurements and estimation of human cell survival for heavy-ion beams. Radiat. Res. 166, 629–638. https://doi.org/10.1667/RR0536.1.
Kellerer, A.M., 1981. Criteria for the equivalence of spherical and cylindrical proportional counters in microdosimetry. Radiat. Res. 86, 277–286.
Knoll, G., 2010. Radiation Detection and Measurements, fourth ed. John Wiley & Sons, Inc.
Kreiner, A.J., Bergueiro, J., Cartelli, D., Baldo, M., Castell, W., Gomez Asoia, J., Padulo, J., Suárez Sandín, J.C., Igarzabal, M., Erhardt, J., Mercuri, D., Valda, A.A., Minsky, D.M., Debraya, M.E., Somacal, H.R., Capoulat, M.E., Herrera, M.S., del Grosso, M.F., Gagetti, L., Anzorena, M.S., Canepa, N., Real, N., Gun, M., Tacca, H., 2016. Present status of accelerator based BNCT. Rep. Practical Oncol. Radiother. 21, 95–101.
Lindborg, L., Nikjoo, H., 2011. Microdosimetry and radiation quality determinations in radiation protection and radiation therapy. Radiat. Protect. Dosim. 143, 402–408.
Loncol, T., Cosgrove, V., Denis, J.M., Gueulette, J., Mazal, A., Menzel, H.G., Pihet, P., Sabattier, R., 1994. Radiobiological effectiveness of radiation beams with broad LET spectra: microdosimetric analysis using biological weighting functions. Radiat. Protect. Dosim. 52, 347–352.
Lindborg, L., Hultqvist, M., Carlsson Tedgren, A., Nikjoo, H., 2013. Lineal energy and radiation quality in radiation therapy: model calculations and comparison with experiment. Phys. Med. Biol. 58, 3089–3105.
Magrin, G., 2018. A method to convert spectra from slab microdosimeters in therapeutic ion-beams to the spectra referring to microdosimeters of different shapes and materials. Phys. Med. Biol. 63, 215021.
Mazzucconi, D., Bortot, D., Pola, A., Agosteo, S., Pasquato, S., Fazzi, A., Colautti, P., Conte, V., 2018. Monte Carlo simulation of a new TEPC for microdosimetry at nanometric level: response against a carbon ion beam. Radiat. Meas. 113, 7–13.
Mazzucconi, D., Bortot, D., Pola, A., Fazzi, A., Colautti, P., Conte, V., Petringa, G., Cirrone, G.A.P., Agosteo, S., 2019a. Nano-microdosimetric investigation at the therapeutic proton irradiation line of CATANA. Radiat. Meas. 123, 26–33.
Mazzucconi, D., Bortot, D., Agosteo, S., Pola, A., Pasquato, S., Fazzi, A., Colautti, P., Conte, V., Petringa, G., Amico, A., Cirrone, G.A.P., 2019b. Microdosimetry at nanometric scale with an avalanche-confinement TEPC: response against a helium ion beam. Radiat. Protect. Dosim. 183, 177–181.
Mazzucconi, D., Bortot, D., Pola, A., Agosteo, S., Selva, A., Colautti, P., Conte, V., 2020a. An Avalanche confinement TEPC as connecting bridge from micro to nanodosimetry. J. Phys. Conf. 1662, 012023.
Mazzucconi, D., Bortot, D., Martin Rodriguez, P., Pola, A., Fazzi, A., Colautti, P., Conte, V., Selva, A., Agosteo, S., 2020b. A wall-less Tissue Equivalent Proportional Counter as connecting bridge from microdosimetry to nanodosimetry. Radiat. Phys. Chem. 171, 108729.
Mazzucconi, D., Bortot, D., Pola, A., Agosteo, S., 2020c. Numerical modeling of the gas gain of low-pressure Tissue-Equivalent Proportional Counter. Nucl. Instrum. Methods 983, 164601.
Moro, D., Colautti, P., Gualdrini, G., Masi, M., Conte, V., De Nardo, L., Tornielli, G., 2006. Two miniaturised TEPCS in a single detector for BNCT microdosimetry. Radiat. Protect. Dosim. 122, 396–400.
Nikjoo, H., Lindborg, L., 2010. RBE of low energy electrons and photons topical review. Phys. Med. Biol. 55, R65–R109.
Paganetti, H., 2014. Relative biological effectiveness (RBE) values for proton beam therapy. Variations as a function of biological endpoint, dose, and linear energy transfer. Phys. Med. Biol. 59, R419–R472.
Parisi, A., Boogers, E., Struelens, L., Vanhavere, F., 2020. Uncertainty budget assessment for the calibration of a silicon microdosimeter using the proton edge technique. Nucl. Instrum. Methods Phys. Res. Sect. A Accel. Spectrom. Detect. Assoc. Equip. A978, 164449.
Rosenfeld, A.B., Bradley, P.D., Cornelius, I., Allen, B.J., Zaider, M., Maughan, R.L., Yanch, J.C., Coderre, J., Flanz, J.B., Kobayashi, T., 2002. Solid state microdosimetry in hadron therapy. Radiat. Protect. Dosim. 101 (1–4), 431–434.
Prokopovich, D.A., Reinhard, M.I., Cornelius, I.M., Rosenfeld, A.B., 2008. SOI microdosimetry for mixed field radiation protection. Radiat. Meas. 43, 1054–1058.
Rosenfeld, A.B., 2016. Novel. Detectors for silicon based microdosimetry, their concepts and applications. Nucl. Instrum. Methods Phys. Res. A809, 156–170.
Suzuki, M., 2020. Boron neutron capture therapy (BNCT): a unique role in radiotherapy with a view to entering the accelerator-based BNCT era. Int. J. Clin. Oncol. 25, 43–50.
Tran, L.T., Bolst, D., Guatelli, S., Biasi, G., Fazzi, A., Sagia, E., Prokopovich, D.A., Reinhard, M.I., Keat, Y.C., Petasecca, M., Lerch, L.F., Pola, A., Agosteo, S., Matsufuji, N., Jackson, M., Rosenfeld, A.B., 2018. High spatial resolution microdosimetry with monolithic ΔE-E detector on 12C beam: Monte Carlo simulations and experiment. Nucl. Instrum. Methods 887, 70–80.
Tudisco, S., Amorini, F., Cabibbo, M., Di Pietro, A., Franzò, G., Figuera, P., Li, S., Musumarra, A., Papa, M., Pappalardo, G., Percolla, G., Priolo, F., Privitera, V., Rizzo, F., 1996. A monolithic silicon telescope. Nucl. Instrum. Methods A 378, 262–266.
Verona, C., Magrin, G., Solevi, P., Bandorf, M., Marinelli, M., Stock, M., Verona Rinati, G., 2018. Toward the use of single crystal diamond based detector for ion-beam therapy microdosimetry. Radiat. Meas. 110, 25–31.
Waker, A.J., Dubeau, J., Surette, R.A., 2009. The application of micro-patterned devices for radiation protection dosimetry and monitoring. Nucl. Technol. 168, 202–206.
Wroe, A., Schulte, R., Fazzi, A., Pola, A., Agosteo, S., Rosenfeld, A., 2009. RBE estimation of proton radiation fields using a de-E telescope. Med. Phys. 36, 4486–4494.
Zahradnik, I.A., Barberet, P., Tromson, D., De Marzi, L., Pomorski, M.T., 2020. A diamond guard ring microdosimeter for ion beam therapy. Rev. Sci. Instrum. 91, 054102.
Zielczyński, M., Golnik, N., 1994. Recombination index of radiation quality - measuring and applications. Radiat. Protect. Dosim. 52, 419–422.
Zielczyński, M., Golnik, N., Rusinowski, Z., 1996. A computer controlled ambient dose equivalent meter based on a recombination chamber. Nucl. Instrum. Methods A370, 563–567.